Check for updates

Chemistry–A European Journal
Research Article
doi.org/10.1002/chem.202400501
Chemistry Europe
European Chemical Societies Publishing
www.chemeurj.org

A Study on Auto-Catalysis and Product Inhibition: A Nucleophilic Aromatic Substitution Reaction Catalysed within the Cavity of an Octanuclear Coordination Cage

Jack C. Dorrat,[a] Christopher G. P. Taylor,[b] Rosemary J. Young,[a] Atena B. Solea,[b] David R. Turner,[a] Genevieve H. Dennison,*[c, d] Michael D. Ward,*[b] and Kellie L. Tuck*[a]

The ability of an octanuclear cubic coordination cage to catalyse a nucleophilic aromatic substitution reaction on a cavity-bound guest was studied with 2,4-dinitrofluorobenzene (DNFB) as the guest/substrate. It was found that DNFB undergoes a catalysed reaction with hydroxide ions within the cavity of the cubic cage (in aqueous buffer solution, pH 8.6). The rate enhancement of k_{cat}/k_{uncat} was determined to be 22, with cavity binding of the guest being required for catalysis to occur. The product, 2,4-dinitrophenolate (DNP), remained bound within the cavity due to electrostatic stabilisation and exerts two apparently contradictory effects: it initially auto-catalyses the reaction when present at low concentrations, but at higher concentrations inhibits catalysis when a pair of DNP guests block the cavity. When encapsulated, the UV/Vis absorption spectrum of DNP is red-shifted when compared to the spectrum of free DNP in aqueous solution. Further investigations using other aromatic guests determined that a similar red-shift on cavity binding also occurred for 4-nitrophenolate (4NP) at pH 8.6. The red-shift was used to determine the stoichiometry of guest binding of DNP and 4NP within the cage cavity, which was confirmed by structural analysis with X-ray crystallography; and was also used to perform catalytic kinetic studies in the solution-state.

Introduction

The development of coordination cages that can bind guests within their cavities or on their surfaces has generated applications in guest reaction catalysis,[1] guest absorption and separation,[2] and molecular sensing.[3] We have developed and evaluated cubic $[M_8L_{12}]^{16+}$ coordination cages that can bind a range of guests and have catalytic capabilities. The ligands in these $[M_8L_{12}]^{16+}$ cages are based on a 1,5-naphthalene-diyl core bearing two pendant chelating pyrazolyl-pyridine units. The ligands each coordinate to two M^{2+} centres that define the vertices of the cage; accordingly, each ligand spans an edge of the M_8 cage (Figure 1).[4] The cubic cage **H** has a cavity volume of approximately 400 Å^3, and according to the 55% rule proposed by Rebek,[5] the optimal size of guest to bind within this cavity in solution is just over 200 Å^3. A wide range of organic guests of this general size have been identified,[6] and the strongest binding constants, of up to 10^6 M^{-1}, in aqueous solutions are observed when the guest fills the cavity to this optimal volume. In the solid state we sometimes observe stacked pairs of bound guests,[7] resulting in much higher cavity occupancies approaching 90%, but such structures are unlikely to dominate in solution.

[a] Dr. J. C. Dorrat, Dr. R. J. Young, Ass. Prof. Dr. D. R. Turner, Prof. K. L. Tuck
School of Chemistry
Monash University
Melbourne, VIC, 3800, Australia
E-mail: Kellie.Tuck@monash.edu

[b] Dr. C. G. P. Taylor, Dr. A. B. Solea, Prof. M. D. Ward
Department of Chemistry
University of Warwick
Coventry, CV4 7AL, UK
E-mail: M.D.Ward@warwick.ac.uk

[c] Dr. G. H. Dennison
CBRN Defence, Sensors and Effectors Division
Defence Science and Technology Group
Fishermans Bend, VIC, 3207, Australia

[d] Dr. G. H. Dennison
Electro Optics Sensing and Electromagnetic Warfare, Sensors and Effectors Division
Defence Science and Technology Group
Edinburgh, SA, 5111, Australia
E-mail: Genevieve.Dennison@defence.gov.au

Supporting information for this article is available on the WWW under https://doi.org/10.1002/chem.202400501

© 2024 The Authors. Chemistry - A European Journal published by Wiley-VCH GmbH. This is an open access article under the terms of the Creative Commons Attribution Non-Commercial NoDerivs License, which permits use and distribution in any medium, provided the original work is properly cited, the use is non-commercial and no modifications or adaptations are made.

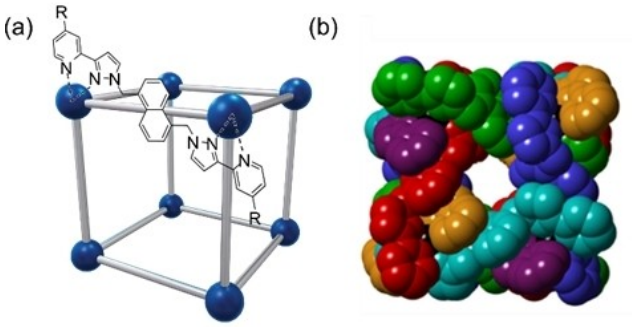

Figure 1. The structure of the $[M_8L_{12}]^{16+}$ cage (**H**, R=H and **H^w**, R=CH_2OH) emphasising (a) the cubic array of Co^{2+} metal ions shown as blue spheres (M) connected by the bridging ligands (L), and (b) the space filling model showing the hollow cavity for guest binding.[4]

© 2024 The Authors. Chemistry - A European Journal published by Wiley-VCH GmbH

Catalysis with our coordination cages occurs firstly *via* binding of the guest into the central cavity or (if it does not fit in the cavity) at the exterior surface, which is driven, in water, by the hydrophobic effect in both cases. Upon binding, the guest is co-localised with the cage counterions, which cluster around the cage due to its 16+ charge. Depending on which guest and which counterion are present, this guest binding can result in either efficient catalysed hydrolysis (of up to k_{cat}/k_{uncat} = 2×10^5, pD 8.5 for benzisoxazole) of specific guests;[8] or their preservation (of up to *ca* 12-fold longer half-life for sarin) due to protection from the bulk environment.[9]

During these studies we have found that the nature of the cage counterion is as important in influencing catalysis as it is in the binding of the substrate itself.[8,10] The counterions of the as-synthesised cage **H** are BF_4^-, but for studies in water, exchange to the Cl^- counterion is often used to enable solubilisation. Under weakly basic conditions, partial anion exchange to hydroxide occurs, and the electrostatically-driven accumulation of hydroxide ions around the cage results in a much higher local pH (>5 pH units increase experienced by a cavity-bound guest) when compared to the aqueous bulk, with the high local concentration of HO^- ions resulting in catalysed hydrolysis or base-mediated reactions of the guest.[9,11] We have also investigated a variety of other counterions in crystallographic studies of salts of the $[M_8L_{12}]^{16+}$ cage, such as NO_3^-, ClO_4^-, BPh_4^-, PF_6^-, SO_4^{2-} and $CF_3SO_3^-$.[4,10,12] These counterions always bind within the portals on the cage surface surrounding the cavity. As a result, both the cavity and surface of the cage have been shown to contribute to catalysis;[11] we note that the interactions responsible for neutral guest binding (predominantly hydrophobic) and anion binding (predominantly electrostatic) can be considered as orthogonal.[12b]

An isostructural analogue of the **H** cage, $\mathbf{H^W}$, bears water-solubilising hydroxymethyl groups on its exterior surface (R= $-CH_2OH$, Figure 1) and catalyses reactions in the same way as the unsubstituted cage **H**. We previously reported that the Kemp elimination reaction of benzisoxazole was catalysed by $\mathbf{H^W}$, where guest binding occurs within the cavity and then the guest reacts with hydroxide counterions located around the cage surface, likely in the surface portals ($k_{cat}/k_{uncat}=2\times10^5$, pD 8.5).[8] The anionic product, 2-cyanophenolate, is ejected from the cage due to its structural change and increased hydrophilicity which makes it preferentially solubilised within the polar aqueous bulk.[4,8] For larger guests, such as nitrobenzisoxasole ($\mathbf{H^W}$, k_{cat}/k_{uncat} of *ca.* 8.5, pH 7.0),[10] some organophosphates (**H**, 2,2-dichlorovinyl dimethyl phosphate, k_{cat}/k_{uncat} of 14, pD 7.7; **H**, 4-nitrophenyl dimethyl phosphate, k_{cat}/k_{uncat} of 11, pD 7.8),[11b] and diacetyl fluorescein ($\mathbf{H^W}$, k_{cat}/k_{uncat} of *ca.* 50),[11a] we found that their reactions with hydroxide were catalysed on the exterior surface of the cage. Whilst guest binding associated with the hydrophobic cage exterior surface is weaker and non-specific compared to cavity-binding, catalysis still occurs because the guests remain exposed to a shell of hydroxide ions, around the cationic cage surface, which are located close to the guests.

Following our previous studies, we wanted to expand our range of study of the reaction types that can be catalysed by these cages, in particular to determine if they can catalyse nucleophilic substitution reactions (S_NAr) of aromatic guests using the HO^- counterion. For this purpose, the substrate 2,4-dinitrofluorobenzene (DNFB) was selected, as it can undergo a S_NAr reaction with HO^-, forming 2,4-dinitrophenolate (DNP) and fluoride ions, a process which can be easily monitored and screened using UV/Vis spectroscopy. The aromaticity of DNFB was expected to facilitate guest binding to the coordination cages both *via* the hydrophobic affect and π-π/CH-π interactions. The $-NO_2$ groups of DNFB act to accelerate its reaction with HO^-, due to its reaction intermediate being stabilised by the Meisenheimer effect (Scheme 1).

We hypothesised that upon binding of DNFB in the cage cavity, its reaction with hydroxide ions would be catalysed by the high local concentration of HO^- anions in a manner similar to our previous examples. The product DNP is in its anionic state under the conditions tested (pH 8.6; pK_a of DNPH is 4.1) and it was hypothesised that ejection of the anion from the cavity due to preferential solvation in the aqueous bulk would enable catalytic turnover. The absorption spectrum of DNP is distinctly different from that of DNFB due to its low-energy charge-transfer transition, and thus its formation can be monitored by changes in absorbance at wavelengths at or above 370 nm.

Results and Discussion

Catalysis of the S_NAr reaction of DNFB

The rate of formation of DNP from DNFB can be determined using UV/Vis spectroscopic analysis in the region of 370 to 460 nm (Figure 2a).[13] By monitoring the absorbance changes at 400 nm, the rate constant for this first-order reaction in borate buffer (100 mM, pH 8.6) with no cage present (*i.e.* background reaction) was determined to be 0.085 ($\pm$0.004)$\times10^{-5}$ s^{-1} (Figure 2b). However, monitoring the formation of DNP in the presence of $\mathbf{H}\cdot Cl_{16}$[1] was complicated by the fact that the addition of $\mathbf{H}\cdot Cl_{16}$ red-shifted the absorption maximum of DNP from 400 nm to 433 nm (Figure 2c), a phenomenon that we have noted before with a different phenolate-based reaction product.[10] Thus, to quantify DNP formation using UV/Vis

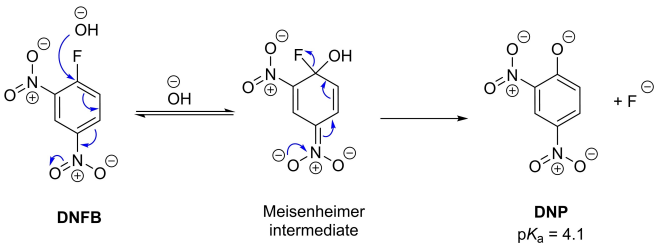

Scheme 1. The S_NAr reaction of 2,4-dinitrofluorobenzene (DNFB) with HO^- to produce 2,4-dinitrophenolate (DNP) and fluoride.

[1] Throughout the manuscript we have referred to the soluble form of the cage as $H\cdot Cl_{16}$, although it is recognised that in solution there will be a mixture of chloride and hydroxide anions at its surface.

© 2024 The Authors. Chemistry - A European Journal published by Wiley-VCH GmbH

15213765, 2024, 27, Downloaded from https://chemistry-europe.onlinelibrary.wiley.com/doi/10.1002/chem.202400501 by Test, Wiley Online Library on [21/05/2024]. See the Terms and Conditions (https://onlinelibrary.wiley.com/terms-and-conditions) on Wiley Online Library for rules of use; OA articles are governed by the applicable Creative Commons License

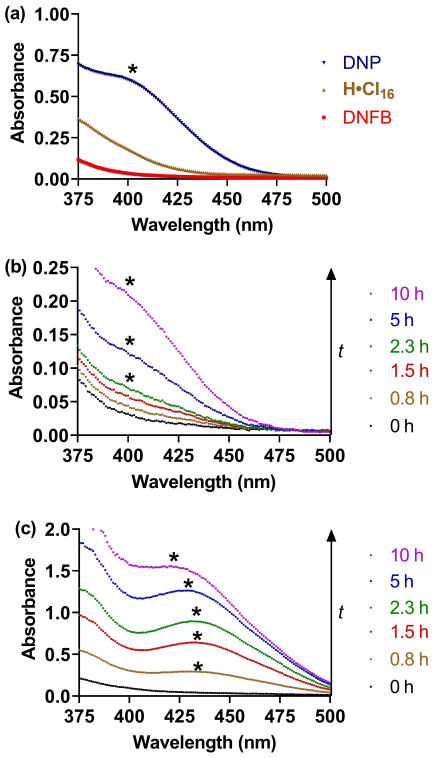

Figure 2. (a) UV/Vis absorption spectra of 0.8 mM DNFB (red), 43 μM DNP (blue) and 75 μM **H**·Cl_{16} (brown); (b) the UV/Vis absorbance changes for conversion of 0.8 mM DNFB to DNP without cage, and (c) with 50 μM **H**·Cl_{16} present; measured over 10 h in 100 mM borate buffer, pH 8.6, λ_{max} denoted by *.

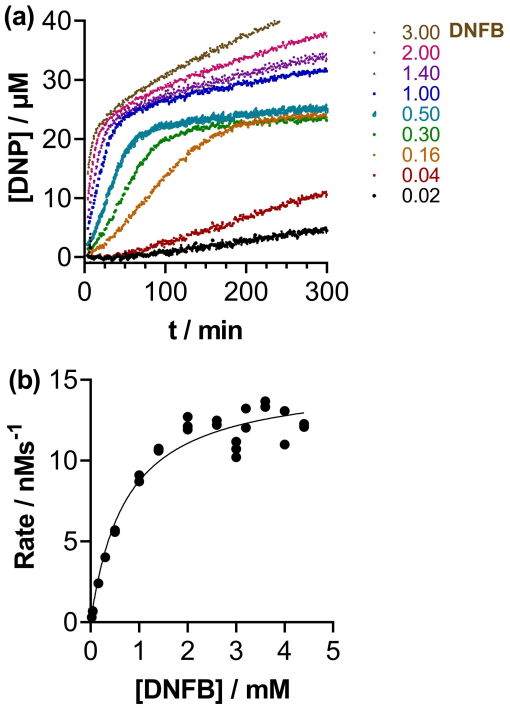

Figure 3. (a) Progress of the S_NAr reaction of DNFB (0.02–4.4 mM) with 0.01 mM **H**·Cl_{16} and (b) the reaction rates vs time with respect to DNFB concentration during the steady state, fitted to a Michaelis-Menten model; determined by UV/Vis analysis, 100 mM borate buffer, pH 8.6 at 450 nm.

spectroscopic analysis, it was necessary to determine the molar extinction coefficients of DNP with varying concentrations of **H**·Cl_{16} (Table S1). The molar extinction coefficients were determined at 450 nm because (i) monitoring DNP formation at this wavelength away from the absorption maximum allowed higher concentrations of DNFB to be measured, and (ii) **H**·Cl_{16} does not absorb at this wavelength. The addition of **H**·Cl_{16} did not red-shift the absorption maximum of DNFB (Figure S1).

The catalysed reaction of DNFB (0.02–4.4 mM) with hydroxide in the presence of **H**·Cl_{16} (0.01 mM) was investigated in aqueous borate buffer (100 mM, pH 8.6). Higher concentrations of DNFB could not be used due to its poor solubility. The presence of the **H**·Cl_{16} clearly catalysed the reaction: at steady state, the reaction followed first-order kinetics with respect to DNFB. With 0.01 mM of **H**·Cl_{16}, the maximum rate (14.3 ± 0.6 nM s^{-1}) was achieved at substrate concentrations of ≥2.0 mM, after which the rate did not increase further (Figure 3a). The first-order rate constant was 1.71×10^{-5} s^{-} [0.16 mM DNFB] – corresponding to a catalytic enhancement of $k_{cat}/k_{uncat} = 22$.

We ascribe this to the catalytic binding site/s of the cage becoming saturated by DNFB, which is in excess of the cage by ≥20:1 at this concentration. Fitting the reaction rates with respect to substrate concentration to a Michaelis-Menten model (Figure 3b), yielded an apparent K_m value of 7.3 (±1.5)$\times10^{-4}$ M.[14]

To confirm that catalysis occurred within the interior cavity of **H**·Cl_{16}, we investigated the reaction in the presence of the smaller tetrahedral cage **T**·Cl_8 ($[Co_4L_6]^{8+}$, Figure 4). The nature of the exterior surface of **T**·Cl_8 is similar to that of the cubic cage, however its cavity is too small to bind DNFB and therefore any catalysis, if it does occur, must be at the exterior surface.[11b] We firstly confirmed that the absorption spectrum of DNP is not red-shifted by the presence of **T**·Cl_8 (Figure S2), in contrast to what we saw with **H**·Cl_{16}, suggesting that this red-shift of the DNP charge-transfer band is a result of cavity binding. The reaction of 0.8 mM DNFB was then monitored with and without the presence of **T**·Cl_8 (0, 0.10 and 0.20 mM) in aqueous buffer (pH 8.6), and unlike with the cubic cage **H**·Cl_{16}, the reaction was only minimally catalysed (Figure S3, <20% increase in reaction rate). This small rate enhancement indicated that the exterior cage surface does impart a minor catalytic influence to the

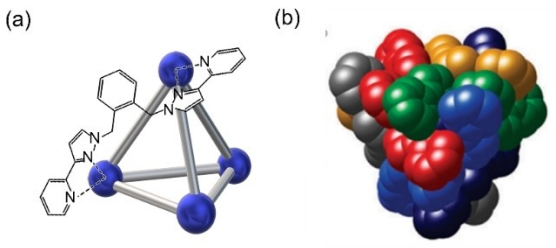

Figure 4. Structure of the $[M_4L_6]^{8+}$ tetrahedral (**T**) cage emphasising (a) the tetrahedral array of Co^{2+} metal ions shown as blue spheres (M) connected by the bridging ligands (L), and (b) the space-filling model highlighting a lack of cavity to guests binding.

© 2024 The Authors. Chemistry - A European Journal published by Wiley-VCH GmbH

15213765, 2024, 27, Downloaded from https://chemistry-europe.onlinelibrary.wiley.com/doi/10.1002/chem.202400501 by Test, Wiley Online Library on [21/05/2024]. See the Terms and Conditions (https://onlinelibrary.wiley.com/terms-and-conditions) on Wiley Online Library for rules of use; OA articles are governed by the applicable Creative Commons License

15213765, 2024, 27, Downloaded from https://chemistry-europe.onlinelibrary.wiley.com/doi/10.1002/chem.202400501 by Test, Wiley Online Library on [21/05/2024]. See the Terms and Conditions (https://onlinelibrary.wiley.com/terms-and-conditions) on Wiley Online Library for rules of use; OA articles are governed by the applicable Creative Commons License

reaction; hydrophobic association of DNFB to the exterior surface of $\mathbf{T}\cdot Cl_8$ exposes the guest to a higher concentration of hydroxide anions surrounding the $\mathbf{T}^{8+}$ cage cation, such that a marginally increased reaction rate is observed. However, the modest enhancement with $\mathbf{T}\cdot Cl_8$ ($k_{cat}/k_{uncat} < 1.2$) does not account for the substantially faster rate of catalysis with the cubic cage $\mathbf{H}\cdot Cl_{16}$ ($k_{cat}/k_{uncat} = 22$), confirming that the reaction of DNFB is catalysed within the cavity of the cubic host.

In addition to the steady-state catalysis as described above, we observed three additional effects which, between them, provide significant insight into the nuances of the catalytic process. Firstly, there was clear inhibition of further catalysis at the point at which formation of DNP product reached 2 equivalents (0.02 mM) (Figure 3a): this unexpected inhibition is a result of two molecules of DNP strongly binding in the cavity as a stacked pair and thereby blocking it (see crystallography section below) – an example of product inhibition. Secondly, autocatalysis was observed in the early stages of the reaction, as shown by a characteristic sigmoidal profile to the reaction progress curves, which means that the product (DNP anion) is facilitating the catalysis, which is therefore not just dependant on the cage,[4] this can be accounted for if we allow that both DNFB (substrate) and DNP (product) can bind in the cavity cooperatively as a hetero-guest pair. Thirdly, the dependence of reaction rate on catalyst concentration (for a fixed substrate concentration) showed, unexpectedly, a maximum and then a *decrease* in reaction rate as more catalyst is added: the origin of this is not immediately obvious but can also be explained as a consequence of the autocatalysis. We return to each of these points in turn.

Firstly, we consider the product inhibition. As noted, the reaction rate dramatically slows following formation of 2.0 equivalents of the reaction products (DNP and fluoride ions) with respect to $\mathbf{H}\cdot Cl_{16}$ (Figure 3a and S4). Thus, both reaction products, DNP and fluoride, were examined separately for their ability to inhibit this reaction.

The addition of fluoride ions (up to 60 mM NaF) to $\mathbf{H}\cdot Cl_{16}$ (0.1 mM) and 0.8 mM DNFB did not alter the reaction rate (Figure S5).[2] However, the addition of the other product DNP (0–2.2 equiv.) significantly inhibited the rate of catalysis, $K_i = 64 \pm 3$ μM (Figure 5 and S6). This finding, in addition to the Job plot analysis (showing formation of a 1:2 **H**:DNP adduct in solution, see below) and the crystallographic studies which show the presence of a stacked pair of DNP guests inside the cavity of **H** (see Figures 7 and 11), supports the conclusion that binding of two molecules of the product DNP within the internal cavity of the cage effectively inhibits the binding of the substrate DNFB, and thus, catalysis no longer occurs. The fact that the catalysed reaction obviously slows down after two equivalents of DNP have accumulated means that binding of the DNP pair must be strong even at the low concentration of **H** used, such that the catalyst cavity is blocked and DNFB can no longer bind.

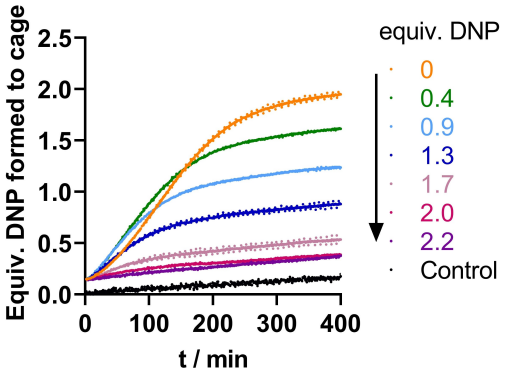

Figure 5. Formation of DNP, presented over time as equivalents of formed DNP with respect to cage, 0.8 mM DNFB, 0.05 mM $\mathbf{H}\cdot Cl_{16}$ and varying amounts of DNP (0, 0.4, 0.9, 1.3, 1.7, 2.0 and 2.2 equiv.); 100 mM borate buffer, pH 8.6 at 450 nm.

Secondly, we consider the autocatalysis in the early stages of the reaction. This requires participation of the DNP anion in a way that facilitates the reaction – which is opposite to the inhibitory effect of a *pair* of DNP anions described above. There is an apparent contradiction here, that small amounts of DNP accelerate the reaction whereas larger amounts inhibit it, and a plausible explanation for this comes from the fact that a DNP anion inside the cavity has scope to stack with a second small aromatic guest (*cf.* the crystal structure) – which might either be second DNP anion (inhibiting the reaction) or a neutral DNFB guest (autocatalysis). Given than DNFB and DNP have essentially the same molecular volume, if there is room for a second DNP anion then there is also room for a DNP/DNFB hetero guest-pair in the cavity.

We suggest a mechanism in which the first DNP anion formed occupies a cage cavity due to the combination of the negative charge and hydrophobicity of the DNP anion. This relatively small guest half-fills the cavity and leaves a space which is ideal for a neutral DNFB to bind, stacked with the DNP anion. Thus, binding of the DNP/DNFB hetero guest-pair is a cooperative process, with a molecule of DNFB binding to $\mathbf{H}\cdot$(DNP) more strongly than it binds to empty **H** because of the favourable π-stacking between DNP and DNFB as well as optimal occupancy of the cage cavity. *The catalytically active species is accordingly not the cage* ***H****, but is the 1:1* $\mathbf{H}\cdot$*(DNP) complex*, to which DNFB binds and undergoes the catalysed reaction: the K_m value of 7.3 (± 1.5)×10^{-4} M, calculated above from the Michaelis-Menten fit (Figure 3b), therefore applies to the binding of DNFB to pre-formed $\mathbf{H}\cdot$(DNP). This explains the autocatalysis, with the reaction rate increasing as the amount of DNP increases and hence the concentration of $\mathbf{H}\cdot$(DNP) increases. Interestingly, and in agreement with this mechanistic hypothesis, upon the addition of DNP (>0.03 mM) to 0.1 mM

[2] The effect of added fluoride varies depending on the reaction under study. In the Kemp elimination reaction using benzisoxazole as substrate, added fluoride slowed down the cage-catalysed reaction by displacing hydroxide from around the cage surface, reducing its local concentration in the vicinity of the substrate.[4] In contrast, we recently observed that fluoride can actually *enhance* cage catalysis for cage-catalysed, base-mediated reactions (*ca.* +70% rate increase observed), suggesting that fluoride ions can accumulate around the cage and act as a base to react with the substrate.[10,11] In this case – reaction of DNFB with hydroxide – there was no significant effect.

© 2024 The Authors. Chemistry - A European Journal published by Wiley-VCH GmbH

$\mathbf{H}\cdot Cl_{16}$ and 0.8 mM DNFB, autocatalysis was no longer observed, further supporting the idea that the presence of DNP allows cooperative binding of DNFB in the cage cavity. This mechanism also explains the third unexpected feature of the catalysis, which is the increase *and then decrease* in reaction rate as more catalyst is added to a fixed amount of substrate. The effect on reaction rates of using 60 μM DNFB with varying concentrations of $\mathbf{H}\cdot Cl_{16}$ (3.3, 6.6, 10, 20, 30, 40, 50 and 75 μM) is shown in Figure 6a. At low concentrations of cage ($\leq$10 μM) the reaction was first order with respect to cage, as expected. As the concentration of cage increases the reaction rate starts to plateau, and by 30 μM concentration of cage (1:2 ratio of host and DNFB) a maximum reaction rate was achieved, with higher concentrations of cage ($\geq$40 μM) actually leading to the reaction rate diminishing (Figure 6b).

The autocatalysis mechanism just presented, based on cooperative formation of a $\mathbf{H}\cdot$(DNP)(DNFB) complex, provides an explanation for this unexpected behaviour. At low concentrations of $\mathbf{H}\cdot Cl_{16}$ we see the expected first-order dependence of reaction rate on catalyst concentration: when catalyst concentration is very low the amount of active catalyst $\mathbf{H}\cdot$(DNP) is limited by [**H**], and more $\mathbf{H}\cdot$(DNP) can form when there is more **H** present. However, when the concentration of **H** becomes larger the amount of $\mathbf{H}\cdot$(DNP) becomes limited by the amount of DNP present: we reach a point where additional **H** is irrelevant and the reaction rate no longer increases. Eventually, the large excess of free **H** binds some DNFB to give a non- or (weakly−) catalytic species, effectively removing DNFB from the productive catalytic cycle, and this effect will increase, slowing down the reaction: effectively, **H** becomes competitive with $\mathbf{H}\cdot$(DNP) for binding of DNFB when [**H**] is high.

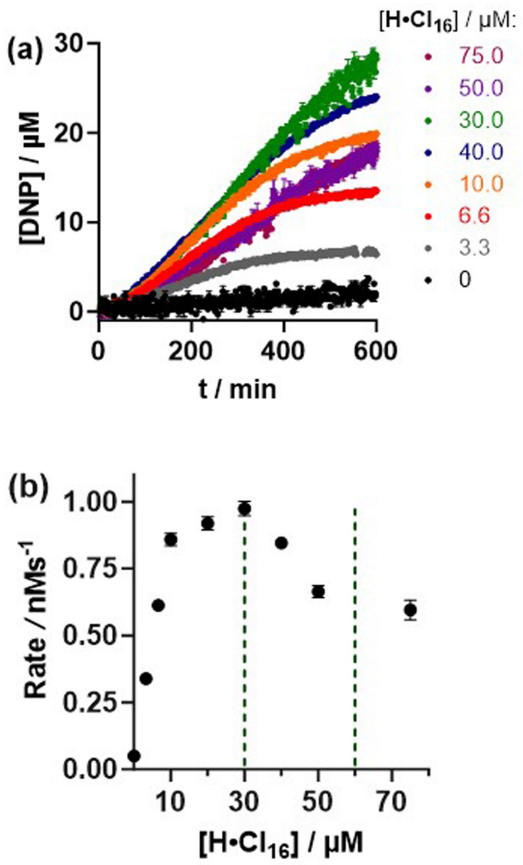

Figure 6. (a) Catalysed conversion of 60 μM DNFB in the presence of $\mathbf{H}\cdot Cl_{16}$ (0, 3.3, 6.6, 10, 20, 30, 40, 50 and 75 μM), and (b) the rate of catalysis during steady state with varying concentration of $\mathbf{H}\cdot Cl_{16}$; 100 mM borate buffer, pH 8.6, n = 2.

Formation of a cage·$(DNFB)_2$ complex could be possible, but if this formation constant is significantly less than for the hetero-pair [cage·DNP·DNFB], for simple electrostatic reasons, then it is insignificant. We note that neutral guests generally do not show cooperativity in binding when two can be accommodated and have $K_2 < K_1$ [7], thus binding of a neutral DNFB pair would not be significant except at very high concentrations. The importance of the negative charge of DNP on facilitating guest binding is shown by the fact the DNP pair bind more strongly than the hetero-pair DNP·DNFB (which explains the observed inhibitory effect), so it reasonably follows that the neutral DNFB pair will bind more weakly again and not contribute significantly to the catalysis.

Whilst product inhibition during catalytic reactions is a common occurrence, in our system, catalysis of DNFB halts in the presence of two equivalents of DNP which form a strongly-binding pair blocking the cavity. Although binding of the DNP pair is, in principle, a reversible equilibrium, the strong binding under the conditions used effectively makes the inhibition irreversible, a rarely seen phenomenon.[15] This is in contrast to the work by Reek and co-workers,[16] and Bergman, Raymond and co-workers,[17] who both observed reversible product inhibition. In a follow-up report by Bergman, Raymond, Toste and co-workers, product inhibition was avoided by addition of maleimide, resulting in a follow-on reaction of the initially-generated product with the added maleimide to give a more weakly binding cycloadduct which vacated the active site, facilitating catalytic turnover.[18] Our data strongly suggests that formation of $\mathbf{H}\cdot(DNP)_2$ prevents any further catalysis, a finding that is further supported by the experiments described below.

Investigating the UV/Vis red-shift of phenolate guests

This is the second time that we have observed a red-shift in the absorption maximum of a guest molecule on binding into the cavity of $\mathbf{H}\cdot Cl_{16}$. We earlier reported that binding of the 2-cyano-4-nitrophenolate anion undergoes a red-shift of its absorption maximum following addition of $\mathbf{H}\cdot Cl_{16}$, with no further red-shift observed after the addition of *ca.* 0.3 equiv. of $\mathbf{H}\cdot Cl_{16}$.[10] From this it was concluded that approximately three guest molecules bound to a single cage molecule, implying that – for this specific guest – surface-binding rather than cavity-binding was occurring.[10] We were therefore interested, given that DNP as guest exhibits similar spectroscopic behaviour, to investigate the extent to which this spectroscopic change allows determination of both host/guest stoichiometry and the guest binding mode, and the results of these experiments provide indirect evidence for the mechanism proposed above.

© 2024 The Authors. Chemistry - A European Journal published by Wiley-VCH GmbH

15213765, 2024, 27, Downloaded from https://chemistry-europe.onlinelibrary.wiley.com/doi/10.1002/chem.202400501 by Test, Wiley Online Library on [21/05/2024]. See the Terms and Conditions (https://onlinelibrary.wiley.com/terms-and-conditions) on Wiley Online Library for rules of use; OA articles are governed by the applicable Creative Commons License

The absorbance of a solution of 0.04 mM DNP was measured in the presence of increasing amounts of **H**·Cl_{16} (0–2.0 equiv., Figure 7). The absorbance changes at 450 nm, with respect to the molar concentrations of cage and substrate, were used to construct a Job plot (Figure 7 insert). The maximum occurred at a concentration of 2.0 equivalents (67% mole fraction) of DNP, indicating the formation of an $\mathbf{H}_1$:$\mathbf{G}_2$ complex. This ratio is consistent with cavity binding, as the exterior surface is large enough to bind more than two guests.[12a] We also know from previous crystallographic studies that many small aromatic guests can bind inside the cavity of **H** as stacked pairs;[7,14a] and indeed the crystallographic studies discussed below, support formation of an $\mathbf{H}_1$:$\mathbf{G}_2$ complex (see Figure 11). This guest binding mode is also in agreement with the outcome of the catalysis studies above, that concluded that 2 equivalents of the product DNP prevent the binding of DNFB and thereby inhibits the cage catalysed reaction (Figure 5).

We extended our investigation to other related guests which may undergo a UV/Vis red-shift in their lowest-energy electronic transition on binding to **H**·Cl_{16}, by examining the absorption spectra of a range aromatic guests with varying functional groups (including a nitro substituent in different positions) with and without the presence of 0.1 mM **H**·Cl_{16} in aqueous buffer (pH 8.6, Figure S7). However, determination of a red-shift was necessarily limited to guests with absorption maxima at longer wavelengths than the strong cage absorption ($\lambda \geq 350$ nm). As shown in Figure 8, 4-nitrophenolate (4NP) also demonstrated an absorption red-shift in the presence of **H**·Cl_{16}. Changes in absorbance at 450 nm, at different mole fractions of host and guest, were used to constructed a Job plot (Figure 8 insert): as with DNP, this demonstrated a maximum at a concentration of 2.0 equiv. of 4NP. This confirmed the formation of a $\mathbf{H}_1$:$\mathbf{G}_2$ complex, a stoichiometry which is consistent with cavity binding as a stacked pair.

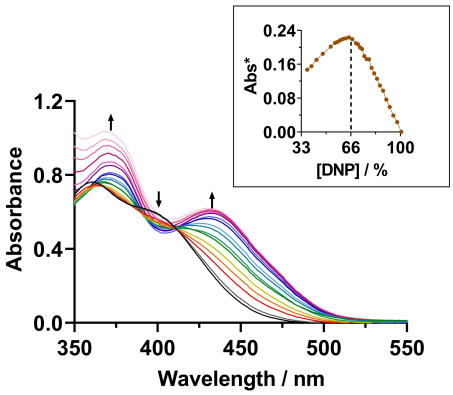

Figure 7. UV/Vis spectra of 0.04 mM DNP with increasing amounts of **H**·Cl_{16} (0 to 2.0 equiv.); insert: Job plot at 450 nm in 100 mM borate buffer, pH 8.6.

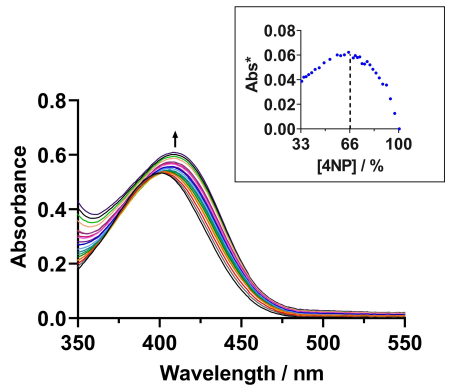

Figure 8. UV/Vis spectra of 0.04 mM 4NP with increasing amounts of **H**·Cl_{16} (0 to 2.0 equiv.); insert: Job plot at 450 nm in 100 mM borate buffer, pH 8.6.

^{1}H-NMR binding studies

Having identified that DNP and 4NP can bind in the cavity of **H** as pairs, their binding constants in the cavity of **H**·Cl_{16} were determined using a conventional ^{1}H-NMR spectroscopic titration study. The ^{1}H-NMR spectrum of 0.2 mM **H**·Cl_{16} was measured with varied concentrations of DNP (0–1.0 mM) or 4NP (0–3.0 mM) in borate buffered D_2O (pD 8.6). For DNP, as the concentration was increased, new ^{1}H-NMR resonances were observed for the cage, indicating slow exchange between free and bound DNP on the NMR timescale (Figure 9). Concentrations of 0.4 mM–1.0 mM of DNP (i.e. greater than 2.0 equiv. per cage) provided no further changes in the ^{1}H-NMR resonances, and guest binding was therefore deemed complete. Utilising the knowledge from the UV/Vis spectroscopic red-shift on DNP binding and the catalysis studies above, that a $\mathbf{H}_1$:$\mathbf{G}_2$ complex with DNP is formed, the binding constant for the formation of this complex (under conditions with a concentration of 1:1.5 host and guest) was calculated as $K_{12} = 1.9\ (\pm 0.2) \times 10^5\ M^{-2}$ (Table 1). As the catalytic studies showed, upon formation, DNP remains within the cavity and once 2.0 equivalents bind the catalytic reaction is completely inhibited. The $\mathbf{H}_1$:$\mathbf{G}_1$ complex was not observable, implying cooperative binding with $K_2 > K_1$ as the first DNP guest provides π-stacking for the second, and hence K_1 could not be determined. We note that the increase in hydrophilicity of anionic DNP compared to the neutral substrate DNFB is not sufficient for it to leave the cavity of **H**·Cl_{16} and transfer to the aqueous phase, a discussion we return to later. Analysis of the binding constant could not

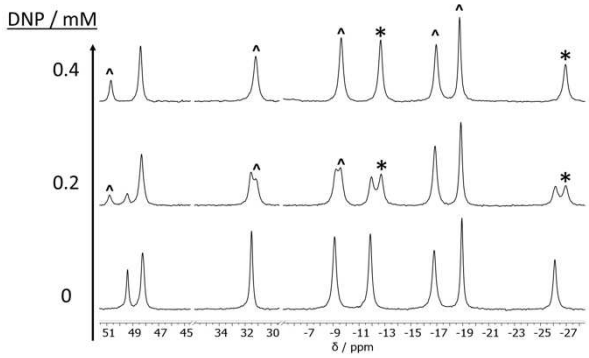

Figure 9. Representative ^{1}H-NMR spectra of 0.2 mM **H**·Cl_{16} with DNP (0, 1.0, 2.0 equiv.) in borate buffer (pD 8.6, 100 mM). Resonances due to the host: guest complexes are labelled ^ or *, those used to calculate binding constants are labelled *.

© 2024 The Authors. Chemistry - A European Journal published by Wiley-VCH GmbH

15213765, 2024, 27, Downloaded from https://chemistry-europe.onlinelibrary.wiley.com/doi/10.1002/chem.202400501 by Test, Wiley Online Library on [21/05/2024]. See the Terms and Conditions (https://onlinelibrary.wiley.com/terms-and-conditions) on Wiley Online Library for rules of use; OA articles are governed by the applicable Creative Commons License

15213765, 2024, 27, Downloaded from https://chemistry-europe.onlinelibrary.wiley.com/doi/10.1002/chem.202400501 by Test, Wiley Online Library on [21/05/2024]. See the Terms and Conditions (https://onlinelibrary.wiley.com/terms-and-conditions) on Wiley Online Library for rules of use; OA articles are governed by the applicable Creative Commons License

Table 1. Binding constants for Host:Guest binding to **H**·Cl_{16}.

Entry	Substrate	[**H**·Cl_{16}]/ mM	[Substrate]/ mM	*K* (error)
a	DNFB	0.01	0–3.0	*app* $K_m = 7.3$ $(\pm 1.5)\times10^{-4}$ M[a]
b	DNP	0.2	0–1.0	$K_{12} = 1.9$ $(\pm 0.2)\times10^{5}$ M^{-2} [b]
c	4NP	0.2	0–3.0	$K_1 = 654$ (12) M^{-1} [c], $K_2 = 1170$ (84) M^{-1} [c] $K_{12} = 7.6$ $(\pm 0.6)\times10^{5}$ M^{-2}

[a] Reaction rates with respect to substrate concentration to a Michaelis-Menten model, determined by UV/Vis spectroscopic analysis. [b] Binding constant determined using a ^{1}H-NMR spectroscopic titration study, slow exchange. [c] Binding constants determined using a ^{1}H-NMR spectroscopic titration study, fast exchange.

be undertaken with DNFB due to the occurrence of catalysis as soon as DNFB and **H**·Cl_{16} are combined.

Addition of 4NP (0–3.0 mM) to 0.2 mM **H**·Cl_{16} resulted in ^{1}H-NMR spectroscopic shifts consistent with binding of guests inside a paramagnetic cavity in fast exchange with the host on the NMR timescale (Figure 10). The addition of more 4NP (10 equiv.) resulted in negligible additional shifts of the resonances. With the knowledge from the UV/Vis absorption study, showing a red-shift on 4NP binding, that a **H**$_1$:**G**$_2$ complex with 4NP is formed, the NMR spectral shifts were fit to a 1:2 host:guest model using Bindfit,[19] to give the binding constants of $K_1 = 654 \pm 12$ M^{-1} and $K_2 = 1171 \pm 84$ M^{-1} and thus $K_{12} = 7.6$ $(\pm 0.6)\times10^{5}$ M^{-2} (Table 1). Thus, calculation of the interaction parameter ($\alpha = 4\,K_2/K_1$) results in a number greater than 1, which confirms positive cooperative binding of the second guest molecule, as we also noted for DNP and also suggested for the DNP/DNFB hetero-guest pair.

The molecular volumes of 4NP and DNP were calculated to be 113 Å^3 and 136 Å^3 respectively.[20] When considering the "55% rule" proposed by Rebek,[5] the fractional occupancies of the cavity are 55% and 66% respectively for these **H**$_1$:**G**$_2$ complexes, approximately within the scope of the Rebek 'rule' of *ca.* 55 ± 9% cavity occupancy being optimal. As we have noted before in crystallographic studies, π–π stacking between aromatic guests can allow a pair of guests to generate high occupancies when bound the cage cavity.[7] Thus, two independent sets of measurements on a related pair of cooperatively-bonding guests, both of which just about fall within the Rebek optimal range of 55 ± 9% for the pair and give △G values of 30 kJ/mol and 34 kJ/mol (300 K) for the cooperative binding events, is consistent and reassuring, and we note that the guest that binds slightly more strongly (DNP over 4NP) is the one with the higher surface area, a key driver for the hydrophobic effect.[6b]

Additionally, during NMR analysis we noted that the chemical environments for cage protons associated with the formation of host·guest complexes of **H**·Cl_{16} with 4NP and DNP were identical as shown by the pattern of chemical shift (12, −16, −18 and −26 ppm, Figure S8), supporting the idea that both guests bind in the same location within the cage cavity.

Crystallographic studies

To further investigate the guest binding of DNFB, DNP, and 4NP to the cage **H** (used as its tetrafluoroborate salt, due to crystallinity and established experimental procedures)[7,10,11] crystallographic studies on the host:guest complexes were performed. X-ray quality crystals of **H**·$(BF_4)_{16}$ with DNP and 4NP as guests were obtained using our previously reported method,[7] which follows the 'crystal sponge' method initially reported by Fujita.[21] This was achieved by soaking crystals of **H**·$(BF_4)_{16}$ in concentrated methanolic solutions of DNPH and 4NPH, hence under forcing conditions. Attempts to obtain a crystal structure of **H**·$(BF_4)_{16}$ with DNFB were unsuccessful due to poor crystallinity after soaking.

For the structure with DNP (Figure 11a), a stacked pair of DNP guests is confirmed inside the cavity of **H**·$(BF_4)_{16}$. Each guest has a site occupancy of 0.5, indicating that on average 50% of the cages contained a stacked pair of DNP guests, confirming that binding two DNP molecules inside the cavity is possible. The two guests are crystallographically equivalent and related by an inversion centre, and are therefore parallel with a

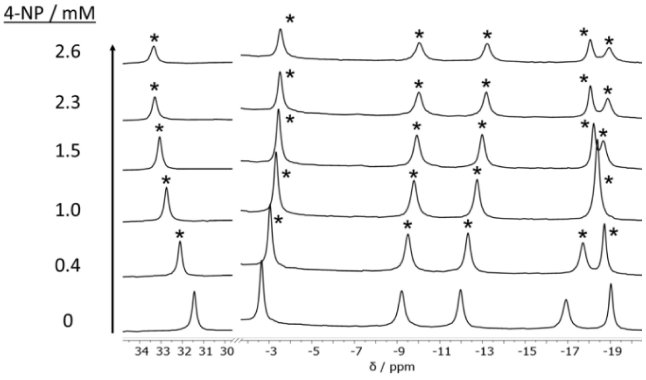

Figure 10. Representative ^{1}H-NMR spectra of 0.2 mM **H**·Cl_{16} with 4NP (0–2.6 mM) in borate buffer D_2O (pD 8.6, 100 mM). Resonances due to host:guest complexes are labelled *.

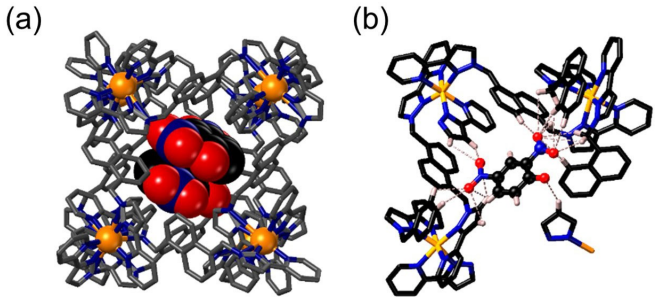

Figure 11. Two views of the crystallographically determined structure of **H**·$(BF_4)_{16}$·2(DNP) (CCDC #2293143); (a) the host is shown as wireframe and the guests as van der Waals radius, (b) showing hydrogen bond interactions of one guest with the inner cage; C = grey/black, O = red, N = blue, Co^{2+} = orange, H = pink.

© 2024 The Authors. Chemistry - A European Journal published by Wiley-VCH GmbH

distance of 3.34 Å between the planes which indicates π–π stacking.[3]

Co-localised within the cavity are two water molecules (site occupancy of 0.5). Additionally, two DNP molecules per cage complex were observed interacting with the exterior surface, each refining to a site occupancy of 0.75. Structural analysis indicated that the encapsulated DNP guests are held in position by 20 hydrogen bond interactions (average D···A distance of 2.83 ± 0.21 Å, Table S2), between either OH (or O^-) and NO_2 moieties of DNP, and CH moieties of the interior of the cage surface (Figure 11b). The structural analysis supports the findings of the solution state studies that concluded that two molecules of DNP bind within the cavity, as shown by the observations that (i) the red-shift of DNP is complete once two molecules are present within the cavity, and (ii) two molecules of DNP within the cavity inhibited cavity-based catalysis of DNFB. We hypothesise that the cooperative guest binding observed in the solution state is derived from both a combination of a DNP pair filling the cavity to the optimal volume, and additionally due to stabilising π–π interactions between both guests within the cage cavity.

The crystal structure of $\mathbf{H}\cdot(BF_4)_{16}$ with 4NP presented many similarities to that of the $\mathbf{H}\cdot(BF_4)_{16}\cdot$2DNP complex. Two molecules of 4NP (each with a site occupancy of 1) were confirmed to be encapsulated within cavity (Figure 12a). Additionally, two non-encapsulated 4NP molecules per cage complex were observed bound to the exterior surface (each with a site occupancy of 0.5). Each cavity-bound 4NP molecule is held in position by 26 hydrogen bonds (average D···A distance of 3.36 ± 0.48 Å, Table S2) interactions between either the OH (or O^-) and NO_2 moieties of the guest and with the CH moieties of the interior of the cage (Figure 12b). The two encapsulated 4NP guests are related by inversion and so are parallel, with a distance of 3.45 Å between the planes indicating π–π interactions. We suggest that these π–π interactions reinforce the cooperative guest binding in the solution state. Any electrostatic repulsion between stacked anions will be mitigated by the head-to-tail arrangement which puts formal negative charges at opposite ends, as observed in the X-ray crystallographic analysis. This structural analysis supports the solution-state Job plot analysis, which concluded that two molecules of 4NP can bind within the cage cavity in solution.

Conclusions

In conclusion, we have shown that the cubic cage $\mathbf{H}\cdot Cl_{16}$ catalyses the S_NAr reaction of DNFB in borate buffer (pH 8.6, 100 mM) with a catalytic rate enhancement k_{cat}/k_{uncat} of 22. The smaller tetrahedral cage, $\mathbf{T}\cdot Cl_8$ whose cavity is not large enough to host DNFB, did not significantly catalyse the S_NAr reaction of DNFB, which confirmed that this reaction is catalysed primarily within the cavity of $\mathbf{H}\cdot Cl_{16}$. DNP both autocatalyses and self-inhibits the catalysis of DNFB, accelerating the reaction its early stages by encouraging formation of a catalytically-active $\mathbf{H}\cdot$(DNP)(DNFB) species, but stopping catalysis once two equivalents of DNP have allowed formation of $\mathbf{H}\cdot(DNP)_2$ which prevents further substrate binding. UV/Vis spectroscopic analysis revealed that DNP undergoes a red-shift of its low-energy charge-transfer transition upon binding to $\mathbf{H}\cdot Cl_{16}$. Further inquiry with other aromatic guests determined that the red-shift also occurred for 4NP at pH 8.6. Analysis of these red-shifts of DNP and 4NP allowed us to conclude that these guests bind within the cavity of $\mathbf{H}\cdot Cl_{16}$, with formation of $\mathbf{H}_1$:$\mathbf{G}_2$ (H = host, G = guest) complexes. Structural analysis of $\mathbf{H}\cdot Cl_{16}$ with DNP and 4NP performed *via* the 'crystal sponge' method, confirmed the conclusions of the solution-based analyses regarding cage/guest stoichiometries and demonstrated two molecules of DNP and 4NP binding within the cavity of the cage in each case. The fractional occupancies of the cavity, with two guests of DNP or 4NP, are 55% and 66% respectively, which is within the Rebek optimal range. The additional electrostatic stabilisation that a pair of cavity-bound anions (DNP or 4NP) encounter inside a 16^+ host results in stronger cavity binding than the neutral guest DNFB. The spectroscopic red-shift in guest absorbance has proved to be a useful tool for investigating the stoichiometry of binding of guests in these cages and may become more widely applicable in the future.

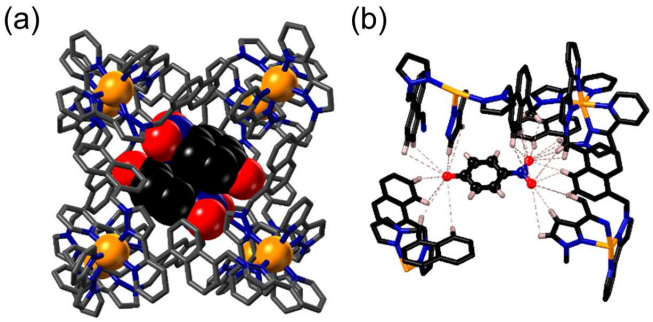

Figure 12. Two views of the crystallographically determined structure of $\mathbf{H}\cdot(BF_4)_{16}\cdot$2(4NP) (CCDC #2293150); (a) the host shown as wireframe and the guests van der Waals radius, (b) showing hydrogen bond interactions of one guest with the inner cage; C = grey/black, O = red, N = blue, Co^{2+} = orange, H = pink.

Experimental

Materials and methods

The preparation of $\mathbf{H}\cdot Cl_{16}$ for solution studies was as previously described.[22] 2,4-Dinitrofluorobenzene (DNFB) (99%), 4-nitrophenol (4NPH) (98%), dinitrophenol (DNPH) (>98%) and cycloundecanone (98%) were purchased from Sigma-Aldrich, and were used without further purification. The absence of DNP impurity in DNFB was confirmed *via* the absence of free F^- ions using ^{19}F-NMR

[3] An alternative possibility on simple stoichiometric grounds is that every cage contains one DNP guest, with them located randomly in one of two off-centre positions such that the superposition coincidentally gives the appearance of a stacked pair with a perfect geometric arrangement, but this is chemically very unlikely: there is no reason why one guest molecule would be located off-centre in this way. Other related structures we have reported have stacked pairs in which fractional occupancies of individual guests are >0.5 confirming the presence of two guest molecules in the same cavity.

© 2024 The Authors. Chemistry - A European Journal published by Wiley-VCH GmbH

15213765, 2024, 27, Downloaded from https://chemistry-europe.onlinelibrary.wiley.com/doi/10.1002/chem.202400501 by Test, Wiley Online Library on [21/05/2024]. See the Terms and Conditions (https://onlinelibrary.wiley.com/terms-and-conditions) on Wiley Online Library for rules of use; OA articles are governed by the applicable Creative Commons License

15213765, 2024, 27, Downloaded from https://chemistry-europe.onlinelibrary.wiley.com/doi/10.1002/chem.202400501 by Test, Wiley Online Library on [21/05/2024]. See the Terms and Conditions (https://onlinelibrary.wiley.com/terms-and-conditions) on Wiley Online Library for rules of use; OA articles are governed by the applicable Creative Commons License

spectroscopic analysis prior to use. The concentration of DNP stock solutions was confirmed using the extinction coefficient in 100 mM borate buffer, pH 8.6.

UV/Vis experiments were performed using a BMG Lab Tech Spectrostar Nano spectrometer cuvette and plate reader measuring at scanning intervals of 1 nm between 260–600 nm, with an incubating temperature set to 27 °C. Thermo Fisher NUNC 96 microplates were used with a volume of 250 μL and a pathlength of 8.36 mm, or quartz cuvettes were used with volumes 2.5–3 mL and a pathlength of 10.0 mm. Red-shift analysis involving the titration of DNP or 4NP into solutions of $\mathbf{H}\cdot Cl_{16}$ were performed in quartz cuvettes with volumes of 2.5–3 mL. All other UV/Vis experiments were performed using NUNC 96 microplates with volumes of V = 250 μL. Spectra were baselined using the corresponding blank.

NMR spectra were recorded on a Bruker DRX400 spectrometer equipped with a 5 mm BBFO probe, operating at 400 MHz (^{1}H) or 377 MHz (^{19}F). Paramagnetic proton nuclear magnetic resonance (^{1}H paramagnetic NMR) were recorded using a spin-echo pulse sequence, over a spectral range of −130 ppm to +150 ppm. The probe temperature was set to 298 K, and standard processing parameters were used for ^{1}H or ^{19}F-NMR spectra. Line broadening was set to 20 Hz for ^{1}H paramagnetic processing. The chemical shifts (δ) are reported in ppm and were referenced to the residual solvent signals (^{1}H).

Solutions of guests were prepared in the appropriate buffer and diluted to the desired concentrations. Due to its instability, solutions of DNFB were prepared in buffer as needed and used immediately.

Extinction coefficients

The extinction coefficients of DNP, with and without $\mathbf{H}\cdot Cl_{16}$ were determined in triplicate at 450 nm using the Beer Lambert law ($A = \varepsilon\iota c$).

UV/Vis spectroscopic analysis

The concentration of DNP from the S_NAr reaction was determined using the absorbance at 450 nm and the extinction coefficient for the conditions (Table S1). The absorbance of the controls was subtracted prior to each calculation.

Determination of rate constants

The rate of reaction was calculated from the change in concentration of DNP during the steady state of reaction *via* the absorbance change at 450 nm. The first-order rate constants (k_1) were calculated from $\ln[DNFB] = k_1 t$, where $[DNFB] = [DNFB_{initial}] - [DNP]$, using GraphPad Prism software version 9.3.1.

Job plot analysis

To solutions of either 4NP or DNP (0.04 mM) in borate buffer (100 mM, pH 8.6) in a quartz cuvette (V = 2.5 mL) was added buffered mixtures of 4NP (0.04 mM) with $\mathbf{H}\cdot Cl_{16}$ (0.35 mM) or DNP (0.04 mM) with $\mathbf{H}\cdot Cl_{16}$ (0.31 mM) respectively. The UV/Vis spectra were acquired 10 seconds post addition and mixing. The concentrations during these experiments for DNP were (0, 1.2, 2.4, 3.7, 4.9, 6.1, 7.3, 8.5, 9.7, 10.9, 12.1, 13.3, 14.4, 15.6, 16.8, 17.9, 19.2, 21.5, 23.8, 26.0, 28.3, 30.5, 32.8, 35.0, 39.4, 48.7, 57.7, 66.4 and 75.0 μM), and for 4NP were (0, 1.4, 2.8, 4.1, 5.5, 6.8, 8.1, 9.4, 10.8, 12.0, 13.3, 14.6, 15.9, 17.1, 18.6, 19.6, 22.7, 25.7, 28.6, 31.5, 38.5, 45.2, 51.6, 57.8, 63.7, 69.3, 74.8, 80.0, 85.0 μM). The Job plots were obtained by plotting **Abs*** as a function of the molar ratio of guest:cage, using the wavelength of 450 nm. To account for the changing substrate + cage concentration, **Abs*** was calculated, where ΔAbs is the change in absorbance at 450 nm of the guest associated with the red-shift:

$$\mathbf{Abs}^* = \Delta Abs/\Sigma[guest] \text{ and } [\mathbf{H}\cdot Cl_{16}]/\Sigma_{initial}[guest] \text{ and } [\mathbf{H}\cdot Cl_{16}]$$

$$\Delta Abs = Absorbance^{guest+cage} - Absorbance^{guest}$$

Determination of binding constants

Solutions of $\mathbf{H}\cdot Cl_{16}$ (0.2 mM) with 4NP (0.1, 0.2, 0.4, 1.0, 1.5, 2.0, 2.3, 2.59, and 2.90 mM) or DNP (0.1, 0.2, 0.3, 0.4, 1.0, and 5.0 mM) were prepared in D_2O (pD 8.6, 100 mM borate buffer) and the resulting ^{1}H paramagnetic NMR spectrum was acquired.

At high DNP guest concentrations (0.3 mM DNP, host:guest ratio of 1 : 1.5) it was assumed that the dominant species is $H_1\cdot G_2$. Thus, the binding constant K_{12} was calculated using the following equation:

$$K_{12} = [H_1 \cdot G_2]/[H] \times [G]^2$$

For 4NP fast guest exchange was observed. The ^{1}H-NMR spectral shifts of $\mathbf{H}\cdot Cl_{16}$ resonances initially at: −19, −17, −12, −9, −3, 31 and 42 ppm were fit to a 1 : 2 host:guest binding isotherm to yield the K_1 and K_2 binding constants using Bindfit.[19] The fits can be found on the Bindfit website at http://app.supramolecular.org/bindfit/view/3df52dc6-1172-4fc8-9f5d-874711a7ce27

Crystallography studies

Crystals of $\mathbf{H}\cdot(BF_4)_{16}$ were prepared as previously described and were suitable for single-crystal X-ray diffraction.[23] The crystals were soaked in a solution containing excess amounts of either DNPH or 4NPH in methanolic mother liquor from the solvothermal growth, for a time period of 24 h. Crystals were transferred to Fomblin oil before they were mounted and flash frozen under liquid nitrogen for storage and transported for analysis. Data collection was performed in Experiment Hutch 1 of the I19 beamline at the UK Diamond Light Source synchrotron.[24] The structures were solved using Olex2 with SHELXT structure solution program using Intrinsic Phasing and refined with SHELXL refinement package using Least Squares Minimisation.[25] Excess solvent molecules and BF_4 counter-ions which could not be modelled due to disorder, for the structure of $\mathbf{H}\cdot(BF_4)_{16}\cdot$DNP were removed using the 'SQUEEZE' function in the PLATON software,[26] and for the structure of $\mathbf{H}\cdot(BF_4)_{16}\cdot$DNP were removed using solvent masking in Olex2 which is based on the 'BYPASS' routine.[27] CrystalMaker was used to construct the figures. Information of crystal properties, data collection and refinement details associated with the structures are in the supporting information CIF.[28]

Supporting Information

Electronic supporting information available: supporting tables and figures, CIF for CCDC #2293143 and #2293150.

© 2024 The Authors. Chemistry - A European Journal published by Wiley-VCH GmbH

15213765, 2024, 27, Downloaded from https://chemistry-europe.onlinelibrary.wiley.com/doi/10.1002/chem.202400501 by Test, Wiley Online Library on [21/05/2024]. See the Terms and Conditions (https://onlinelibrary.wiley.com/terms-and-conditions) on Wiley Online Library for rules of use; OA articles are governed by the applicable Creative Commons License

Acknowledgements

The authors acknowledge the support of the School of Chemistry, Monash University; the Australian Defence Science and Technology Group; and the Department of Chemistry, University of Warwick. We thank the Australian Department of Defence for research funding, the Universities of Warwick and Monash University for a 'Monash/Warwick Alliance' Accelerator Grant to MDW, KLT, GHD and DRT, the Royal Society for an International Exchange Grant IES/R3/170177 to MDW and KLT, and Monash University, School of Chemistry for a Dean's Scholarship to JCD. We thank the Swiss National Science Foundation for an Early Postdoc Mobility fellowship (project P2FRP2/199583) to ABS. We thank the Diamond Light Source for beamtime (proposal CY25064) and the staff of beamtime I19 for assistance. Open Access publishing facilitated by Monash University, as part of the Wiley - Monash University agreement via the Council of Australian University Librarians.

Conflict of Interests

The authors declare no conflict of interest.

Data Availability Statement

The data that support the findings of this study are available in the supplementary material of this article.

Keywords: supramolecular chemistry · host-guest systems · coordination cage · catalysis · crystallography

[1] a) T. Murase, S. Horiuchi, M. Fujita, *J. Am. Chem. Soc.* **2010**, *132*, 2866; b) I. Sinha, P. S. Mukherjee, *Inorg. Chem.* **2018**, *57*, 4205; c) Y. Fang, J. A. Powell, E. Li, Q. Wang, Z. Perry, A. Kirchon, X. Yang, Z. Xiao, C. Zhu, L. Zhang, F. Huang, H.-C. Zhou, *Chem. Soc. Rev.* **2019**, *48*, 4707; d) R. Ham, C. J. Nielsen, S. Pullen, J. N. H. Reek, *Chem. Rev.* **2023**, *123*, 5225.
[2] a) D. F. Sava, V. C. Kravtsov, J. Eckert, J. F. Eubank, F. Nouar, M. Eddaoudi, *J. Am. Chem. Soc.* **2009**, *131*, 10394; b) S. Mukherjee, A. V. Desai, S. K. Ghosh, *Coord. Chem. Rev.* **2018**, *367*, 82; c) D. Zhang, T. K. Ronson, Y.-Q. Zou, J. R. Nitschke, *Nat. Chem. Rev.* **2021**, *5*, 168.
[3] a) K. Ono, M. Yoshizawa, M. Akita, T. Kato, Y. Tsunobuchi, S.-I. Ohkoshi, M. Fujita, *J. Am. Chem. Soc.* **2009**, *131*, 2782; b) W. P. Lustig, S. Mukherjee, N. D. Rudd, A. V. Desai, J. Li, S. K. Ghosh, *Chem. Soc. Rev.* **2017**, *46*, 3242; c) C. Guo, A. C. Sedgwick, T. Hirao, J. L. Sessler, *Coord. Chem. Rev.* **2021**, *427*, 213560.
[4] W. Cullen, A. J. Metherell, A. B. Wragg, C. G. P. Taylor, N. H. Williams, M. D. Ward, *J. Am. Chem. Soc.* **2018**, *140*, 2821.
[5] S. Mecozzi, J. Rebek, *Chem. Eur. J.* **1998**, *4*, 1016.
[6] a) M. D. Ward, C. A. Hunter, N. H. Williams, *Acc. Chem. Res.* **2018**, *51*, 2073; b) S. Turega, W. Cullen, M. Whitehead, C. A. Hunter, M. D. Ward, *J. Am. Chem. Soc.* **2014**, *136*, 8475; c) J. R. Piper, L. Cletheroe, C. G. P. Taylor, A. J. Metherell, J. A. Weinstein, I. V. Sazanovich, M. D. Ward, *Chem. Commun.* **2017**, *53*, 408; d) W. Cullen, K. A. Thomas, C. A. Hunter, M. D. Ward, *Chem. Sci.* **2015**, *6*, 4025; e) W. Cullen, S. Turega, C. A. Hunter, M. D. Ward, *Chem. Sci.* **2015**, *6*, 625; f) A. J. Metherell, W. Cullen, N. H. Williams, M. D. Ward, *Chem. Eur. J.* **2018**, *24*, 1554.
[7] C. G. Taylor, S. P. Argent, M. D. Ludden, J. R. Piper, C. Mozaceanu, S. A. Barnett, M. D. Ward, *Chem. Eur. J.* **2020**, *26*, 3054.
[8] W. Cullen, M. C. Misuraca, C. A. Hunter, N. H. Williams, M. D. Ward, *Nat. Chem.* **2016**, *8*, 231.
[9] J. C. Dorrat, R. J. Young, C. G. P. Taylor, M. B. Tipping, A. J. Blok, D. R. Turner, A. I. McKay, S. Ovenden, M. D. Ward, G. H. Dennison, K. L. Tuck, *Dalton Trans.* **2023**, *52*, 11802.
[10] M. D. Ludden, C. G. Taylor, M. B. Tipping, J. S. Train, N. H. Williams, J. C. Dorrat, K. L. Tuck, M. D. Ward, *Chem. Sci.* **2021**, *12*, 14781.
[11] a) A. B. Solea, B. Suditttapong, C. G. P. Taylor, M. D. Ward, *Dalton Trans.* **2022**, *51*, 11277; b) C. G. P. Taylor, A. J. Metherell, S. P. Argent, F. M. Ashour, N. H. Williams, M. D. Ward, *Chem. Eur. J.* **2020**, *26*, 3065.
[12] a) M. D. Ludden, M. D. Ward, *Dalton Trans.* **2021**, *50*, 2782; b) M. D. Ludden, C. G. P. Taylor, M. D. Ward, *Chem. Sci.* **2021**, *12*, 12640; c) S. Turega, M. Whitehead, B. R. Hall, A. J. H. M. Meijer, C. A. Hunter, M. D. Ward, *Inorg. Chem.* **2013**, *52*, 1122.
[13] R. H. De Rossi, M. Barra, E. B. De Vargas, *J. Org. Chem.* **1986**, *51*, 2157.
[14] a) C. Mozaceanu, A. B. Solea, C. G. P. Taylor, B. Suditttapong, M. D. Ward, *Dalton Trans.* **2022**, *51*, 15263; b) J. S. Train, A. B. Wragg, A. J. Auty, A. J. Metherell, D. Chekulaev, C. G. P. Taylor, S. P. Argent, J. A. Weinstein, M. D. Ward, *Inorg. Chem.* **2019**, *58*, 2386.
[15] T. K. Piskorz, V. Martí-Centelles, R. L. Spicer, F. Duarte, P. J. Lusby, *Chem. Sci.* **2023**, *14*, 11300.
[16] P. Dydio, R. J. Detz, B. de Bruin, J. N. H. Reek, *J. Am. Chem. Soc.* **2014**, *136*, 8418.
[17] C. J. Hastings, M. D. Pluth, R. G. Bergman, K. N. Raymond, *J. Am. Chem. Soc.* **2010**, *132*, 6938.
[18] C. M. Hong, M. Morimoto, E. A. Kapustin, N. Alzakhem, R. G. Bergman, K. N. Raymond, F. D. Toste, *J. Am. Chem. Soc.* **2018**, *140*, 6591.
[19] http://supramolecular.org, accessed August 21, 2023.
[20] https://www.molinspiration.com/cgi/properties, accessed November 06, 2023.
[21] a) M. Hoshino, A. Khutia, H. Xing, Y. Inokuma, M. Fujita, *IUCrJ* **2016**, *3*, 139; b) K. Rissanen, *Chem. Soc. Rev.* **2017**, *46*, 2638.
[22] a) M. Whitehead, S. Turega, A. Stephenson, C. A. Hunter, M. D. Ward, *Chem. Sci.* **2013**, *4*, 2744; b) G. D. Jackson, M. B. Tipping, C. G. P. Taylor, J. R. Piper, C. Pritchard, C. Mozaceanu, M. D. Ward, *Chemistry* **2021**, *3*, 1203.
[23] I. S. Tidmarsh, T. B. Faust, H. Adams, L. P. Harding, L. Russo, W. Clegg, M. D. Ward, *J. Am. Chem. Soc.* **2008**, *130*, 15167.
[24] D. R. Allan, H. Nowell, S. A. Barnett, M. R. Warren, A. Wilcox, J. Christensen, L. K. Saunders, A. Peach, M. T. Hooper, L. Zaja, *Crystals* **2017**, *7*, 336.
[25] a) O. V. Dolomanov, L. J. Bourhis, R. J. Gildea, J. A. K. Howard, H. Puschmann, *J. App. Crystallogr.* **2009**, *42*, 339; b) G. Sheldrick, *Acta Crystallogr. Sect. A* **2008**, *64*, 112; c) G. Sheldrick, *Acta Crystallogr. Sect. C* **2015**, *71*, 3; d) G. Sheldrick, *Acta Crystallogr. Sect. A* **2015**, *71*, 3.
[26] A. Spek, *Acta Crystallogr. Sect. C* **2015**, *71*, 9.
[27] P. Van der Sluis, A. Spek, *Acta Crystallogr. Sect. A* **1990**, *46*, 194.
[28] Deposition numbers #2293143 (for $\mathbf{H}\cdot(BF_4)_{16}\cdot 2(DNP)$) and #2293150 (for $\mathbf{H}\cdot(BF_4)_{16}\cdot 2(4NP)$) contain the supplementary crystallographic data for this paper. These data are provided free of charge by the joint Cambridge Crystallographic Data Centre and Fachinformationszentrum Karlsruhe Access Structures service.

Manuscript received: February 3, 2024
Accepted manuscript online: March 3, 2024
Version of record online: March 26, 2024

© 2024 The Authors. Chemistry - A European Journal published by Wiley-VCH GmbH